PCCP

Accepted Manuscript

ROYAL SOCIETY OF CHEMISTRY

www.rsc.org/pccp

Journal Name

ARTICLE TYPE

Cite this: DOI: 10.1039/xxxxxxxxxx

Magneto-optical properties of ABC-stacked trilayer graphene

Yi-Ping Lin,[a] Chiun-Yan Lin,*[a‡1] Yen-Hung Ho,[b] Thi-Nga Do,[a] Ming-Fa Lin*[a‡2]

Received Date
Accepted Date

DOI: 10.1039/xxxxxxxxxx

www.rsc.org/journalname

The generalized tight-binding model is developed to investigate magneto-optical absorption spectra of ABC-stacked trilayer graphene. The absorption peaks can be classified into nine categories of inter-Landau level optical excitations, including three intra-group and six inter-group ones. Most of them belong to the twin-peak structures because of the asymmetric Landau level spectrum. The threshold absorption peak only comes from a certain excitation channel, and its frequency is associated with a specific interlayer atomic interaction. The Landau-level anticrossings cause extra absorption peaks. Moreover, a simple relation between the absorption frequency and the field strength is absent. The magneto-optical properties of ABC-stacked trilayer graphene are totally different from those of AAA- and ABA-stacked ones, such as the number, intensity and frequency of absorption peaks.

1 INTRODUCTION

Few-layer graphenes have attracted an abundance of theoretical and experimental investigations since their unique hexagonal symmetry results in such extraordinary electronic properties as a quantum Hall effect[1–3], high electron mobility[4–6], and low-frequency plasma[7,8]. They can be produced successfully by experimental methods including mechanical exfoliation[9–11], chemical vapor deposition[12–15], epitaxial growth of graphene on SiC[16], and Hummer's method[17,18]. Especially, the ABC-stacked graphenes can be readily produced by the first three methods. The low-energy electronic properties can be significantly altered by varying the stacking configurations[19,20], the layer number[21–23], and the external magnetic and electric fields[23–28]. The magnetic quantization can induce three kinds of highly degenerate Landau levels (LLs) and thus abundant magneto-optical absorption spectra[29]. In this work, the optical absorption spectra of ABC-stacked trilayer graphene in the presence of a uniform magnetic field ($\mathbf{B} = B_0\hat{z}$) are thoroughly investigated by using the generalized tight-binding model. Furthermore, detailed comparisons with AAA- and ABA-stacked trilayer graphenes are discussed.

The rich electronic properties of trilayer graphenes are dominated by the stacking configuration. The AAA stacking has three pairs of linear bands[30], and the ABA one possesses two pairs of parabolic and one pair of linear energy bands[31]. These bands can be respectively considered as a superposition of three monolayer graphenes and a combination of a monolayer and AB-stacked bilayer graphene. On the other hand, the ABC stacking exhibits one pair each of a partial flat, a sombrero-shaped and a parabolic band[32]. This is in sharp contrast to the individual bands of the sub-systems. The magnetic quantization in their LL energy spectra and wavefunctions is quite different amongst them. Each LL in the AAA stacking is well described by a simple-mode harmonic function, and the energy spectra of three LL groups are proportional to $\sqrt{B_0}$[33]. Such characteristics are also revealed in one LL group of the ABA-stacked trilayer graphene[34]. The other two LL groups possess AB-stacked bilayer-like characteristics, such as linear B_0-dependent energy spectra and special LL modes near the Fermi level (E_F). However, a simple relation between the energy spectrum and B_0 is absent in the ABC stacking. Induced by certain interlayer atomic interactions, the LL anticrossings appear in three different manners with respect to ABC, ABA, and AAA stackings: often, seldom, and never.

Some theoretical and experimental research studies on the magneto-optical properties of few-layer graphenes. The theoretical calculations only focus on the AA- and AB-stacked systems. In AA-stacked N-layered graphene, there are N categories of absorption peaks for the N groups of LLs[33,35], in which only the intra-group LL excitations exist, whereas the inter-group ones are absent. The AB-stacked bilayer graphene presents four categories of absorption peaks[36,37]. However, in the trilayer one only the intra-group excitation channels due to the first LL group have been investigated[38]. Some predicted results, e.g., square-root or linear B_0-dependent frequencies and a selection rule of $\Delta n = \pm 1$, have been confirmed by transmission[39–41] and Raman scattering spectroscopy[42–44]. The distinct stacking configurations are ex-

[a] Department of Physics, National Cheng Kung University, 701 Tainan, Taiwan.
[b] National Tsing Hua University, 300 Hsinchu, Taiwan.
‡1 E-mail: l28981084@mail.ncku.edu.tw
‡2 E-mail: mflin@mail.ncku.edu.tw

pected to enrich the magneto-absorption spectra.

The generalized tight-binding model, based on the subenvelope functions of distinct sublattices, is utilized to study the magneto-absorption spectra of ABC-stacked trilayer graphene over a wide frequency range. The relationships between the spatial distributions of the LL wavefunctions and the available optical excitation channels will be explored. Calculations on the number, structure, frequency and intensity of the absorption peaks are performed in detail. This work shows that three groups of LLs can generate nine categories of absorption peaks, six of which result from intergroup LL excitations, while the other three arise from intra-group ones. Only a few absorption peaks exhibit single-peak behavior, while the majority of the others display twin-peak structures. The peak frequencies monotonously rise with an increase of the magnetic field except for those of the extra peaks that present a discontinuous B_0 dependence due to the intergroup LL anticrossing. Moreover, the irregular frequency-dependent absorption rates are also obtained. The predicted results could be verified by optical spectroscopy methods[45–49]; detailed examinations of the obtained spectra are useful in identifying the stacking configurations among trilayer graphene systems.

2 Model

The magneto-electronic spectrum of the ABC-stacked trilayer graphene is calculated by the generalized tight-binding model. The six intra- and inter-layer atomic interactions ($\beta_0 = 3.16$ eV, $\beta_1 = 0.36$ eV, $\beta_2 = -0.01$ eV, $\beta_3 = 0.32$ eV, $\beta_4 = 0.03$ eV, and $\beta_5 = 0.013$ eV) are taken into account[32]. The vector potential due to a uniform perpendicular magnetic field induces a periodical phase; therefore, the enlarged rectangular unit cell includes $12R_B$ atoms ($R_B = hc/eB_0$). The $12R_B \times 12R_B$ Hamiltonian can be more efficiently solved by the band-like matrix being obtained by the rearrangement of $12R_B$ tight-binding functions. The eigenfunction can be expressed as

$$|\Psi_k^{c,v}\rangle = \sum_{l=1}^{3}\sum_{j=1}^{2R_B}(c_{A_{jk}^l}|A_{jk}^l\rangle + c_{B_{jk}^l}|B_{jk}^l\rangle),$$

where the superscripts c and v represent respectively a conduction and a valence state; $\sum_{j=1}^{2R_B} c_{A_{jk}^l}|A_{jk}^l\rangle$ and $\sum_{j=1}^{2R_B} c_{B_{jk}^l}|B_{jk}^l\rangle$ denote the subenvelope functions on the six distinct sublattices. B_j^1, B_j^2, and B_j^3, which are shown in Fig. 1, are subjected to the same lattice environments as A_j^3,A_j^2, and A_j^1, respectively. The quantum number $(n_l^{c,v})$ of each LL can be characterized by the number of nodes in the dominating subenvelope wavefunctions.

The occupied Landau state is excited to the unoccupied one with the same wavevector. The unit vector of the electric polarization $\hat{\mathbf{E}}$ is assumed to be along $\hat{y}$. According to Fermi golden rule, the optical absorption function is given by

$$A(\omega) \propto \sum_{c,v,j,j'}\int_{1stBZ}\frac{d\mathbf{k}}{(2\pi)^2}\mid\langle\Psi^c(\mathbf{k},j)|\frac{\hat{\mathbf{E}}\cdot\mathbf{P}}{m_e}|\Psi^v(\mathbf{k},j')\rangle\mid^2 \times Im[\frac{f(E^c(\mathbf{k},j))-f(E^v(\mathbf{k},j'))}{E^c(\mathbf{k},j)-E^v(\mathbf{k},j')-\omega-i\Gamma}], \quad (1)$$

where $f(E^{c,v}(\mathbf{k},j))$ is the Fermi-Dirac distribution function, and Γ is the broadening parameter ($\Gamma \simeq 1$ meV). The intensities of the absorption peaks are mainly determined by the velocity matrix elements in Eq. (1) that relate to the initial state and the final state. Given that the wavevectors are the same, such elements can be calculated by gradient approximation[50].

$$\langle\Psi^c(\mathbf{k},j)|\frac{\hat{\mathbf{E}}\cdot\mathbf{P}}{m_e}|\Psi^v(\mathbf{k},j')\rangle \cong \frac{\partial}{\partial k_y}\langle\Psi^c(\mathbf{k},j)|H|\Psi^v(\mathbf{k},j')\rangle = \sum_{l,l'=1}^{3}\sum_{j,j'=1}^{2R_B}(c_{A_{j,k}^l}^* c_{A_{j',k}^{l'}}\frac{\partial}{\partial k_y}\langle A_{j,k}^l|H|A_{j',k}^{l'}\rangle + c_{A_{j,k}^l}^* c_{B_{j',k}^{l'}}\frac{\partial}{\partial k_y}\langle A_{j,k}^l|H|B_{j',k}^{l'}\rangle$$
$$+c_{B_{j,k}^l}^* c_{A_{j',k}^{l'}}\frac{\partial}{\partial k_y}\langle B_{j,k}^l|H|A_{j',k}^{l'}\rangle + c_{B_{j,k}^l}^* c_{B_{j',k}^{l'}}\frac{\partial}{\partial k_y}\langle B_{j,k}^l|H|B_{j',k}^{l'}\rangle).$$

The approximation has been successfully used in studying other carbon-related systems, e.g., carbon nanotubes[51], graphite[52], and nanographite ribbons[53]. So that, the velocity matrix can be simplified to be the product of three matrices: amplitudes of the initial state, amplitudes of the final state and $\partial H/\partial k_y$ When the velocity matrix element does not vanish, the initial and final states in the product should be the two states corresponding to the nonvanishing hopping integrals. Thus, the in-plane atomic interaction β_0 makes the largest contributions to the optical excitations. Consequently, the Landau modes need to be identical on the same layer for the A (B) sublattice of the initial state and the B (A) sublattice of the final state, a satisfactory condition for the existence of absorption peaks[29]. In other words, the optical transitions are available only when the A and B sublattices have the same mode according to the orthonormal relationship of the subenvelope functions.

3 Results

ABC-stacked trilayer graphene possesses three LL groups, which can be distinguished by the characteristics of the distinct suben-

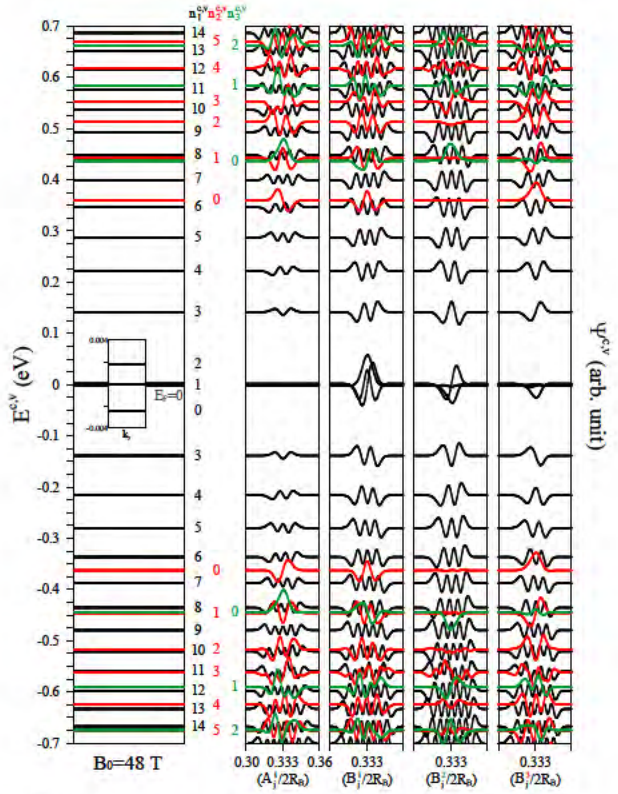

Fig. 1 The three group of Landau levels and their respective subenvelope wavefunctions, B_j^1, B_j^2, and B_j^3, are distinguished by the black, red, and green colors for $B_0 = 48$ T.

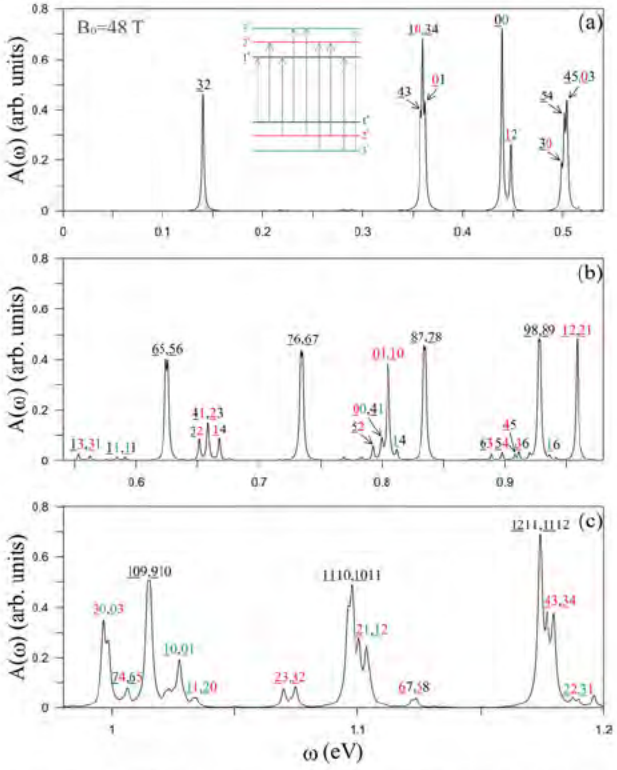

Fig. 2 Optical absorption spectra of ABC-stacked trilayer graphene in (a), (b), and (c) with respect to different frequency ranges for $B_0 = 48T$. The number represents the quantum number of the occupied LL with the underline, and symbolizes the quantum number of the unoccupied LL without the underline. The black, red, and green colors corresponds to the first, second, and third LL groups.

velope wavefunctions. The first, second, and third groups are, respectively, indicated by the black, red, and green colors in Fig. 1 at $B_0 = 48$ T. Their quantum numbers, $n_1^{c,v}$, $n_2^{c,v}$, $n_3^{c,v}$, are characterized by the B_j^1, B_j^3, B_j^2 sublattices, respectively. The spatial distributions of the wavefunctions exhibit symmetric and antisymmetric properties; therefore, they play an important role for the intensity of the optical excitations and the selection rule. The valence and conduction LLs are asymmetric with respect to $E_F = 0$ due to the interlayer atomic interactions, a characteristic being totally different from monolayer graphene. As to the first group, the three LLs of $n_1^v = 0$, $n_1^{c,v} = 1$ and $n_1^c = 2$ spread over a small energy range near E_F where the $n_1^{c,v} = 1$ LL is located at E_F, and the others ($n_1^{c,v}$) commence from 3. The second and the third groups emerge from $|E^{c,v}| \sim 0.36$ eV and ~ 0.45 eV, respectively. The quantum numbers of $n_2^{c,v}$ and $n_3^{c,v}$ both begin from zero. Most of the LLs are well-behaved in the spatial distribution; that is, their quantum numbers can be clearly assigned by the zero-point number of the dominating subenvelope function. On the other hand, some of the LLs are composed of a main and side modes. For example, the $n_3^{c,v} = 1$ subenvelope function in Fig. 1 is mixed with the side mode $n_2^{c,v} = 3$, and vice versa. Also reflected in the LL anticrossings is the fact that the $n_3^{c,v} = 1$ of the third group and the $n_2^{c,v} = 3$ of the second group avoid crossing each other between $B_0 = 40$ T and $B_0 = 60$ T. Such LLs can induce a complicated LL anti-crossing energy spectrum in a certain B_0-range[32] (Fig. 3), they are expected to induce extra magneto-absorption peaks.

The ABC-stacked trilayer graphene exhibits a feature-rich optical absorption spectrum. Three groups of valence LLs can be arbitrarily excited to three groups of conduction LLs ($n_l^v \to n_{l'}^c$), so that all the excitations can be classified into nine categories (three intragroup and six intergroup LL excitations). The optical excitations related to the first, second, and third LL groups are symbolized by the black, red, and green colors in Fig. 2, respectively. The threshold absorption peak, coming from the first category, arises at $\omega = 0.14$ eV for $B_0 = 48$ T as a result of the optical transition from the occupied $n_1^v = 3$ LL to the unoccupied $n_1^c = 2$ LL (denoted $n_1^v n_1^c = \underline{32}$ in Fig. 2(a), where the underline symbol denotes the quantum number of the occupied LL). The mode of the A_j^1 sublattice in the $n_1^v = 3$ LL is identical to that of the B_j^1 sublattice in the $n_1^c = 2$ LL (Fig. 1), a condition satisfying the optical selection rule. Moreover, other prominent peaks successively appear from $\omega = 0.36$ eV. There are two kinds of twin-peak structures in the optical absorption spectrum. One belongs to the same category, and the other is owned by two different categories. Except for the first absorption peak, all the others exhibit the twin-peak structure in the first category, e.g., $n_1^v n_1^c = \underline{43}$ and $n_1^v n_1^c = \underline{34}$, and so forth. The frequency spacing of these twin peaks, induced by the asymmetry between the occupied and the unoccupied LLs, may be observable. Similar twin-peak structures can be observed for the other intragroup excitations $n_2^v \to n_2^c$ and $n_3^v \to n_3^c$, which successively appear from $\omega = 0.80$ eV and $\omega = 1.03$ eV, as shown in Figs. 2(b) and 2(c). The asymmetric LLs cause the optical

excitaions from two different groups of LLs to create the twin-peak structures, in which they include the ($n_1^v \to n_2^c$ & $n_2^v \to n_1^c$), ($n_1^v \to n_3^c$ & $n_3^v \to n_1^c$), and ($n_2^v \to n_3^c$ & $n_3^v \to n_2^c$) excitations. As illustrated, the three absorption peaks denoted ($n_1^v n_2^c = \underline{1}0$ & $n_2^v n_1^c = \underline{0}1$), ($n_1^v n_3^c = \underline{1}1$ & $n_3^v n_1^c = \underline{1}1$), and ($n_2^v n_3^c = \underline{0}0$ & $n_3^v n_2^c = \underline{0}0$) form the twin-peak structures at $\omega = 0.36$ eV, $\omega = 0.58$ eV, and $\omega = 0.80$ eV, respectively. On the other hand, the ABC-stacked trilayer graphene possesses the three particular LLs ($n_1^v = 0$, $n_1^{c,v} = 1$, $n_1^c = 2$) near E_F; therefore, there exist three single-structure absorption peaks ($n_1^v n_1^c = \underline{3}2$, $n_1^v n_3^c = \underline{0}0$, $n_2^v n_1^c = \underline{1}2$). This result is attributed to the Fermi-Dirac distribution and the optical selection rule. It is noteworthy that the intensities of the absorption peaks here are totally different from those in the monolayer graphene. The former vary randomly with rising frequency, while the latter are uniform and independent on the photon frequency. For example, the intensity of $n_1^v n_3^c = \underline{0}0$ at $\omega = 0.44$ eV is higher than that of $n_1^v n_1^c = \underline{3}2$ at $\omega = 0.14$ eV. The main reason is that the inner product of the A_j^1 subevenlope function in $n_3^c = 0$ LL and the B_j^1 subevenlope function in $n_1^v = 0$ LL is larger than that of the A_j^1 subevenlope function in $n_1^v = 3$ LL and the B_j^1 subevenlope function in $n_1^c = 2$ LL, as shown in Fig. 1.

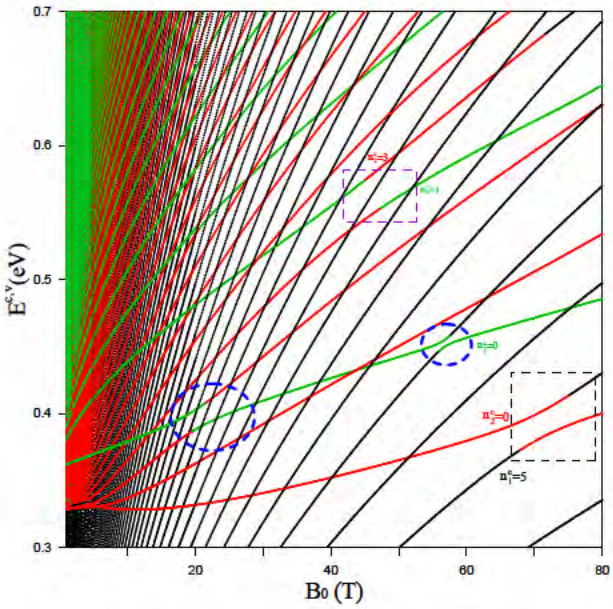

Fig. 3 The B_0 dependence plot of the Landau energies of the ABC-stacked trilayer graphene. Note that the intergroup Landau level anticrossings are marked by the purple and black rectangle, and blue circles.

On the other hand, the magneto-optical spectrum exhibits some unusual absorption peaks. Particular LL anticrossings are revealed in certain magnetic-field ranges, as indicated by the dashed blue circles, and the purple and black rectangles in Fig. 3. The subevenlope wavefunctions, with a continuous change in the anticrossing region, are composed of the main ($n_l^{c,v}$) and side ($n_l^{c,v} \pm 3$) modes[32]. Moreover, their competition plays an important role in generating extra absorption peaks. For example, the two twin-peak structures in Fig. 4, ($n_2^v n_3^c = \underline{3}0$ & $n_3^v n_2^c = \underline{0}3$) and ($n_2^v n_3^c = \underline{2}1$ & $n_3^v n_2^c = \underline{1}2$), are caused by the anticrossing of the $n_2^{c,v} = 3$ and $n_3^{c,v} = 1$ LLs (dashed purple rectangle in Fig. 3). For the initial magnetic field at $B_0 = 30$ T, the absorption intensities are weak because the amplitude of the side mode is small in the Landau wavefunction. The influence of the side mode is getting stronger with increasing B_0; this leads to a rise in intensities of the twin peaks until the field strength passes the anticrossing point at $B_0 \sim 48$ T. After that, the effect of the side mode is reduced and the two anticrossing LLs reverse, i.e., the energy of the $n_2^{c(v)} = 3$ LL becomes higher (lower) than that of the $n_3^{c(v)} = 1$ LL. Therefore, blue- and red-shifts occur in the ($n_2^v n_3^c = \underline{3}0$ & $n_3^v n_2^c = \underline{0}3$) and ($n_2^v n_3^c = \underline{2}1$ & $n_3^v n_2^c = \underline{1}2$) twin-peak structures, respectively (blue rectangle in Fig. 4).

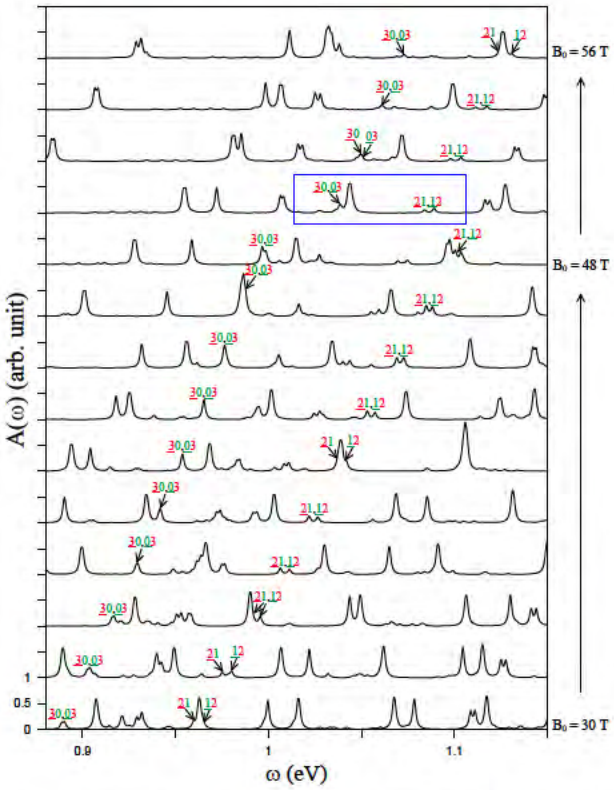

Fig. 4 The progression of the extra peaks from $B_0 = 30$ T to $B_0 = 56T$.

AAA-, ABA-, and ABC-stacked trilayer graphenes differ considerably from one another in terms of the main features of their magneto-absorption spectra, such as the number, intensity, and frequency of absorption peaks. The AAA stacking can be regarded as three layers of a monolayer graphene; therefore, it has only three categories of absorption peaks belonging to the intragroup excitation category[33]. Intergroup excitations are forbidden since all LL wavefunctions are linear symmetric or asymmetric superpositions of the subenvelope wavefunctions in the different layers. The ABA system is expected to possess five categories of absorption peaks, reflecting the fact that it can be regarded as the superposition of a AB-stacked bilayer and a monolayer graphene[36,38]. Obviously, the ABC stacking owns more categories of absorption peaks with their frequencies unable to be interpreted using the independent sub-systems. The extra peaks induced by the LL anticrossings are revealed frequently in the ABC-stacked system, and rarely in the ABA-stacked one; they are absent in the AAA-stacked

one. The intensities of the absorption peaks are non-uniform in the ABA- and ABC-stacked graphene; nevertheless, they are uniform in the AAA stacking, except for the first few peaks in each intragroup excitation category. Moreover, the threshold frequency is lowest for the AAA stacking, which is in accordance with the selection rule. These signatures are helpful in identifying the different stacking configurations from experimental measurements.

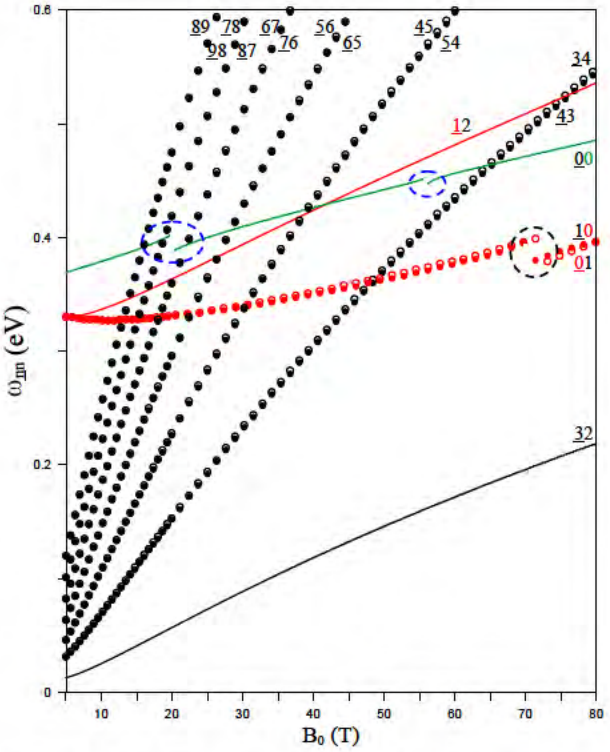

Fig. 5 Field-dependent frequencies of the ABC-stacked trilayer graphene in the low fequency range. The frequencies of the single- and twin-peak structures are plotted by curves and pairs of circles, respectively. The intergroup excitation categories are indicated by the red and green colors, and the intragroup ones are shown by the black color.

The dependence of the low-lying inter-LL absorption peaks on the field strength deserves a closer examination. The intragroup excitation frequencies ($\omega_{\underline{nn}}$) grow quickly with the increment of B_0, as demonstrated in Fig. 5. The relation between $\omega_{\underline{nn}}$ and B_0 can not be described as a simple semi-parabolic ($\sqrt{B_0}$) or linear formula like that in the monolayer or bilayer system[54]. As the field strength is reduced, absorption frequencies approach the threshold frequency $\omega_{\underline{32}}$. At a sufficiently small B_0, the three degenerate LLs at E_F lead to $\omega_{\underline{32}} \sim$10 meV, which corresponds to the energy spacing $\Delta E^{c,v} \sim 2|\beta_2|$ of the first pair of the patial flat bands along the KΓ direction under a zero external field[32]. There exist intergroup absorption peaks in between the intragroup ones, including $\underline{1}0$, $0\underline{1}$, $\underline{0}0$, and $\underline{1}2$. The first three excitations exhibit a non-continuous structure at a certain B_0, mainly owing to the LL anticrossing (Fig. 3). For example, both $\underline{1}0$ and $0\underline{1}$ are interrupted at $B_0 = 70$ T (black rectangle) as a result of the anticrossing of the $n_1^{c,v} = 5$ and $n_2^{c,v} = 0$ LLs (black rectangle in Fig. 3). Likewise, the $\underline{0}0$ absorption peak stops at $B_0 = 20$ T and $B_0 = 55$ T because two LL anticrossings occur (blue circles in Fig. 3). Moreover, the energy spacing of the twin-peak structure is decreased with an increament of the frequency.

Optical spectroscopy methods, including absorption, transmission, reflection, Raman scattering and Rayleigh scattering spectroscopy, have been widely used to study the magneto-properties of graphene-related systems, such as carbon nanotubes, graphene nanoribbons, few-layer graphenes, graphite and graphite intercalation compounds[55–58]; these spectroscopic techniques are also applicable to other few-layer systems, such as MoS_2 [59,60] and silicene[61,62], and topological insulators, such as Bi_2-Se_3 [63]. Previous works have elaborated on the LL excitations associated with the effects of dimensionality, curvature, and boundary conditions. Magneto-absorption/transmission and Rayleigh spectra evidently reveal the Aharonov-Bohn effect and the angular-momentum couplings in carbon nanotubes. On the other hand, in graphene nanoribbons, the first inter-quasi-LL transitions are observed with a substantial deviation arising from an upper-hybrid mode between the LLs and the confined plasmons[64].

In 2D graphene systems, the square-root and linear-dependent B_0 frequencies responsible for massless and massive Dirac-fermions are observed in the infrared transmission spectra of monolayer and AB-stacked bilayer graphenes, respectively. Recently, both kinds of Dirac-fermions have been revealed by magneto-Raman spectroscopy in AB-stacked graphene up to five layers. Furthermore, the two frequency dependencies also appear in the vicinity of the H point and K point of AB-stacked graphite, as demonstrated by respective magneto-absorption/transmission and magneto-reflection spectra. Besides, the latter also shows an optical reflectance associated with LL excitation energies, which can be used to determine the tight-binding parameters of graphite and graphite intercalation compounds[65].

These magneto-optical characteristics of graphene-related systems are attributed to the optical excitations between well-behaved LLs and satisfy the selection rule $\Delta n = \pm 1$. However, in particular for ABC-stacked graphene, twin-peak structures are observed in the nine groups, i.e., three intra-group categories and six inter-group categories. The absorption frequencies follow neither a simple square-root dependence nor a linear dependence. It should be noted that the optical excitations within the anticrossing spectrum lead to a considerable amount of extra peaks, the numbers and intensities of which are significantly increased with LL hybridization. Apparently, the extra peaks are quite different from those of the well-behaved LLs in that they exhibit blue and red shifts during the exchange of anticrossing LLs. The threshold frequency is determined by the vertical next-nearest interlayer atomic interaction $\beta 2$ at a small B_0. The aforementioned absorption spectra features can be verified by optical spectroscopy methods.

4 Conclusion

The generalized tight-binding model is developed to study the magneto-optical properties of ABC-stacked trilayer graphene. It is also useful in understanding the other essential physical properties, e.g., the Coulomb excitations and transport properties. The main characteristics of the absorption spectra are thoroughly in-

vestigated, such as the peak structures, and the number, intensity and frequency of absorption peaks. Deduced from the spatial symmetry of the Landau wavefunctions, the optical selection rule is that the A (B) sublattice of the initial state and the B (A) sublattice of the final state need to have an identical mode for the same layer. The theoretical predictions can be verified by optical spectroscopy methodes.

ABC-stacked trilayer graphene exhibits rather different magneto-absorption spectra than AA- and AB-stacked graphenes. The spectra of AA- and AB-stacked trilayer graphenes possess three and five categories of absorption peaks, which can be, respectively, regarded as a combination result of three monolayer graphenes, and of a monolayer and a bilayer graphenes. However, for ABC-stacked trilayer graphene, the LL transitions are allowed from one of the three valence groups to any of the three conduction groups, leading to a variety of absorption peaks, which are classified into three intra-group and six inter-group categories. Single-peak and twin-peak structures are observed in the magneto-absorption spectra. The former peaks are contributed by the specific excitations from the three LLs in the vicinity of the Fermi level, determining the threshold frequencies for the categories related to the first group. The latter peaks are caused by pairs of excitation channels in the asymmetric LL spectrum. The threshold frequency at a sufficient small B_0 is associated with a specific interlayer atomic interaction. There is absence of a simple relationship between the absorption frequencies and the magnetic field strengths. It should be noted that the hybridized LLs, in particular for the inter-group categories, lead to a considerable amount of extra peaks which exhibit blue and red shifts during a variation of the magnetic field.

This work characterizes the magneto-optical properties of ABC-stacked graphene over a wide range of frequencies. The results can be used to identify the stacking configuration. Furthermore, the generalized tight-binding model can be further devoted to study other two-dimensional materials, such as MoS_2 and silicene[66]. They present an intrinsic bandgap and the electronic dispersion resembles linear dispersion of Dirac fermions. This model can be adapted to the sp3 hybridizations in the buckled structure and accommodate the in uence of external fields and geometric structures.

References

1 C. L. Kane and E. J. Mele, *Physical Review Letters*, 2005, **95**, 226801.
2 W. Zhu, V. Perebeinos, M. Freitag and P. Avouris, *Phys. Rev. B*, 2009, **80**, 235402.
3 E. A. Henriksen, D. Nandi and J. P. Eisenstein, *Phys. Rev. X*, 2012, **2**, 011004.
4 Y. M. Lin, C. Dimitrakopoulos, K. A. Jenkins, D. B. Farmer, H. Y. Chiu, A. Grill and P. Avouris, *Science*, 2010, **327**, 662.
5 K. Nagashio, T. Nishimura, K. Kita and A. Toriumi, Electron Devices Meeting (IEDM), 2009 IEEE International, 2009, p. 1.
6 M. Craciun, S. Russo, M. Yamamoto, J. B. Oostinga, A. Morpurgo and S. Tarucha, *Nature nanotechnology*, 2009, **4**, 383.
7 X. Jiang, *Phys. Rev. B*, 1996, **54**, 13487.
8 J. Y. Wu, S. C. Chen, O. Roslyak, G. Gumbs and M. F. Lin, *ACS nano*, 2011, **5**, 1026.
9 K. F. Mak, M. Y. Sfeir, J. A. Misewich and T. F. Heinz, *Proceedings of the National Academy of Sciences*, 2010, **107**, 14999.
10 M. J. Webb, P. Palmgren, P. Pal, O. Karis and H. Grennberg, *Carbon*, 2011, **49**, 3242.
11 Z. Liu, Q. S. Zheng and J. Z. Liu, *Applied Physics Letters*, 2010, **96**, 201909.
12 J. H. Warner, M. Mukai and A. I. Kirkland, *ACS nano*, 2012, **6**, 5680.
13 A. Obraztsov, E. Obraztsova, A. Tyurnina and A. Zolotukhin, *Carbon*, 2007, **45**, 2017.
14 Z. Y. Juang, C. Y. Wu, A. Y. Lu, C. Y. Su, K. C. Leou, F. R. Chen and C. H. Tsai, *Carbon*, 2010, **48**, 3169.
15 B. Jayasena and S. Subbiah, *Nanoscale Res. Lett*, 2011, **6**, 95.
16 W. Norimatsu and M. Kusunoki, *Phys. Rev. B*, 2010, **81**, 161410.
17 W. S. Hummers Jr and R. E. Offeman, *Journal of the American Chemical Society*, 1958, **80**, 1339.
18 A. Kumarasinghe, L. Samaranayake, F. Bondino, E. Magnano, N. Kottegoda, E. Carlino, U. Ratnayake, A. De Alwis, V. Karunaratne and G. A. Amaratunga, *The Journal of Physical Chemistry C*, 2013, **117**, 9507.
19 Z. Wang, H. Zheng, Q. Shi, J. Chen, J. Yang and J. Hou, *arXiv preprint cond-mat/0703422*, 2007.
20 A. C. Neto, F. Guinea, N. Peres, K. S. Novoselov and A. K. Geim, *Reviews of modern physics*, 2009, **81**, 109.
21 J. Nilsson, A. C. Neto, F. Guinea and N. Peres, *Physical Review B*, 2008, **78**, 045405.
22 B. Partoens and F. M. Peeters, *Phys. Rev. B*, 2007, **75**, 193402.
23 M. Aoki and H. Amawashi, *Solid State Communications*, 2007, **142**, 123.
24 C. H. Lui, Z. Li, K. F. Mak, E. Cappelluti and T. F. Heinz, *Nature Physics*, 2011, **7**, 944.
25 J. H. Ho, Y. H. Lai, Y. H. Chiu and M. F. Lin, *Nanotechnology*, 2008, **19**, 035712.
26 Y. H. Lai, C. P. Chang, J. H. Ho, C. H. Ho and M. F. Lin, *Physics Letters A*, 2008, **372**, 292.
27 C. L. Lu, C. P. Chang, Y. C. Huang, J. H. Ho, C. C. Hwang and M. F. Lin, *Journal of the Physical Society of Japan*, 2007, **76**, 024701.
28 S. Sena, J. M. Pereira Jr, F. M. Peeters and G. Farias, *Physical Review B*, 2011, **84**, 205448.
29 Y. K. Huang, S. C. Chen, Y. H. Ho, C. Y. Lin and M. F. Lin, *Sci. Rep.*, 2014, **4**, 7509.
30 I. Lobato and B. Partoens, *Phys. Rev. B*, 2011, **83**, 165429.
31 S. Latil and L. Henrard, *Physical Review Letters*, 2006, **97**, 036803.
32 Y. P. Lin, J. Wang, J. M. Lu, C. Y. Lin and M. F. Lin, *RSC Adv.*, 2014, **4**, 56552.
33 C. P. Chang, *Journal of Applied Physics*, 2011, **110**, 013725.
34 S. Yuan, R. Roldán and M. I. Katsnelson, *Physical Review B*, 2011, **84**, 125455.

35 R. B. Chen, Y. H. Chiu and M. F. Lin, *Carbon*, 2013, **54**, 268.

36 Y. H. Ho, Y. H. Chiu, W. P. Su and M. F. Lin, *Applied Physics Letters*, 2011, **99**, 011914.

37 Y. H. Ho, Y. H. Chiu, D. H. Lin, C. P. Chang and M. F. Lin, *ACS nano*, 2010, **4**, 1465.

38 S. Berciaud, M. Potemski and C. Faugeras, *Nano letters*, 2014, **14**, 4548.

39 E. Henriksen, P. Cadden-Zimansky, Z. Jiang, Z. Li, L.-C. Tung, M. Schwartz, M. Takita, Y.-J. Wang, P. Kim and H. Stormer, *Physical review letters*, 2010, **104**, 067404.

40 Z. Jiang, E. Henriksen, L. Tung, Y. J. Wang, M. Schwartz, M. Han, P. Kim and H. Stormer, *Physical review letters*, 2007, **98**, 197403.

41 P. Plochocka, C. Faugeras, M. Orlita, M. Sadowski, G. Martinez, M. Potemski, M. Goerbig, J.-N. Fuchs, C. Berger and W. De Heer, *Physical review letters*, 2008, **100**, 087401.

42 C. Faugeras, M. Amado, P. Kossacki, M. Orlita, M. Kühne, A. Nicolet, Y. I. Latyshev and M. Potemski, *Physical review letters*, 2011, **107**, 036807.

43 H. Zhao, Y. C. Lin, C. H. Yeh, H. Tian, Y. C. Chen, D. Xie, Y. Yang, K. Suenaga, T. L. Ren and P. W. Chiu, *ACS nano*, 2014, **8**, 10766.

44 L. Malard, M. Pimenta, G. Dresselhaus and M. Dresselhaus, *Physics Reports*, 2009, **473**, 51.

45 D. Graf, F. Molitor, K. Ensslin, C. Stampfer, A. Jungen, C. Hierold and L. Wirtz, *Nano letters*, 2007, **7**, 238.

46 M. Orlita, C. Faugeras, J. Schneider, G. Martinez, D. Maude and M. Potemski, *Physical review letters*, 2009, **102**, 166401.

47 A. C. Ferrari, J. C. Meyer, V. Scardaci, C. Casiraghi, M. Lazzeri, F. Mauri, S. Piscanec, D. Jiang, K. S. Novoselov, S. Roth and A. K. Geim, *Phys. Rev. Lett.*, 2006, **97**, 187401.

48 S. Wang, R. Wang, X. Liu, X. Wang, D. Zhang, Y. Guo and X. Qiu, *The Journal of Physical Chemistry C*, 2012, **116**, 10702.

49 D. Basov, M. Fogler, A. Lanzara, F. Wang and Y. Zhang, *Reviews of Modern Physics*, 2014, **86**, 959.

50 M. F. Lin and K. W. K. Shung, *Phys. Rev. B*, 1994, **50**, 17744.

51 H. Carmona, A. Geim, A. Nogaret, P. Main, T. Foster, M. Henini, S. Beaumont and M. Blamire, *Phys. Rev. Lett.*, 1995, **74**, 3009.

52 C. P. Chang, C. L. Lu, F. L. Shyu, R. B. Chen, Y. K. Fang and M. F. Lin, *Carbon*, 2004, **42**, 2975.

53 M. Kato, A. Endo, S. Katsumoto and Y. Iye, *Phys. Rev. B*, 1998, **58**, 4876.

54 Y. H. Ho, Y. H. Chiu, J. Wang, D. H. Lin and M. F. Lin, *Japanese Journal of Applied Physics*, 2011, **50**, year.

55 C. Casiraghi, A. Hartschuh, E. Lidorikis, H. Qian, H. Harutyunyan, T. Gokus, K. Novoselov and A. Ferrari, *Nano letters*, 2007, **7**, 2711.

56 Y. Zhang, T. T. Tang, C. Girit, Z. Hao, M. C. Martin, A. Zettl, M. F. Crommie, Y. R. Shen and F. Wang, *Nature*, 2009, **459**, 820.

57 T. Kaplas, A. Zolotukhin and Y. Svirko, *Optics express*, 2011, **19**, 17226.

58 Y. Kim, Y. Ma, A. Imambekov, N. G. Kalugin, A. Lombardo, A. C. Ferrari, J. Kono and D. Smirnov, *Phys. Rev. B*, 2012, **85**, 121403.

59 B. C. Windom, W. Sawyer and D. W. Hahn, *Tribology Letters*, 2011, **42**, 301.

60 H. Li, Q. Zhang, C. C. R. Yap, B. K. Tay, T. H. T. Edwin, A. Olivier and D. Baillargeat, *Advanced Functional Materials*, 2012, **22**, 1385.

61 D. Jose, A. Nijamudheen and A. Datta, *Physical Chemistry Chemical Physics*, 2013, **15**, 8700.

62 E. Cinquanta, F. Scotognella, D. Chiappe, C. Grazianetti, E. Scalise, M. Houssa, M. Fanciulli, C. Vozzi and A. Molle, *Bulletin of the American Physical Society*, 2014, **59**, year.

63 J. Zhang, Z. Peng, A. Soni, Y. Zhao, Y. Xiong, B. Peng, J. Wang, M. S. Dresselhaus and Q. Xiong, *Nano letters*, 2011, **11**, 2407.

64 J. M. Poumirol, W. Yu, X. Chen, C. Berger, W. A. de Heer, M. L. Smith, T. Ohta, W. Pan, M. O. Goerbig, D. Smirnov and Z. Jiang, *Phys. Rev. Lett.*, 2013, **110**, 246803.

65 E. Mendez, T. Chieu, N. Kambe and M. Dresselhaus, *Solid State Communications*, 1980, **33**, 837.

66 G. R. Berdiyorov, M. Neek-Amal, F. M. Peeters and A. C. T. van Duin, *Phys. Rev. B*, 2014, **89**, 024107.